Development and dynamic modeling of a new hybrid thermo-piezoelectric micro-actuator

Micky Rakotondrabe, *member, IEEE* and Ioan Alexandru Ivan, *member, IEEE*

***Abstract*— This paper presents a new hybrid micro-actuator based on the combination of piezoelectric and thermal effects. The proposed actuator can perform both a high stroke coarse positioning through the thermal actuation, and a high resolution fine positioning through the piezoelectric actuation.**

The micro-actuator structure is a unimorph piezoelectric cantilever, which also constitutes a thermal bimorph that is very sensitive to temperature variation. While electrical voltage is used to control the piezoelectric actuation, we use a Peltier module to provide the temperature variation and to control the thermal functioning. In order to understand the behavior of the hybrid actuator, a model is developped. For better precision but at the same time for model simplicity, the thermal part is modeled with the thermal network whereas the Prandtl-Ishlinskii hysteresis approach is used to model the nonlinearity of the piezoelectric part. Finally, a series of experimental results validate the developed model.

***Index Terms*— Hybrid micro-actuator, piezoelectricity, thermal bimorph, unimorph cantilever, dynamic model, thermal network, Prandtl-Ishlinskii hysteresis, nonlinearity.**

I. Introduction

THe micromanipulation and microassembly concern is the manipulation and assembly of functionnal and structured products whose dimensions are less than $1mm$. Nowadays, the degree of miniaturization of many systems and products leads laboratories and industry to use micromanipulation and microassembly tasks. For instance, the assembly of watch microcomponents, 3D MEMS and MOEMS (Micro Opto Electro Mechanical Systems) needs flexible microassembly stations [1] [2]. The aligning of microspectrometer fibers [3] and the manipulation of biological cells [4] [5] also recover from the micromanipulation. Either micromanipulation or microassembly tasks need micromanipulators and microrobots with very high performances: high accuracy, high resolution, high range of positioning and sometimes high response time. This is why these systems are based on smart material actuators instead of actuators with hinges.

One of the most prized smart materials for designing micro-actuators are ceramic piezoelectric materials, especially the PZT family (Lead Zirconate Titanate). They have proved their efficiency in piezogrippers [6] [7], stick-slip micro-actuators [8] [9], and Atomic Force Microscopes (AFM). In fact, piezoelectric materials offer a very high resolution, a high force density and a small response time. In addition, the fact that its input energy is electrical makes it easy to control. As examples, in improved AFMs, piezoelectric actuators can offer subnanometric resolution [10] while in some piezogrippers and piezocantilevers, their settling time is less than $10ms$ [11]. Although they are quick and accurate, the range of deformation of piezoelectric actuators is very limited. In fact, the coupling coefficient of piezoelectric material is weak relative to that of other types of smart materials. The solution of maximizing the output deformation by supplying higher voltage is not convenient as it may cause the material depolarization.

Compared to piezoelectric actuators, thermal actuators are characterized by higher range of deformation. Most designs employ the thermal bimorph cantilever principle which is made up of two different metallic layers. When submitted to a temperature variation, the difference in thermal expansions of the two layers will result in a bending of the cantilever. Provided the resulting large deflection, thermal bimorph actuators are employed to design microgrippers and micropositionning devices [12] [13]. Thermal actuators also include cooling phases, instead of heating ones, such as in [14] where the actuator freezes and creates ice in order to manipulate objects in water media. Unfortunately, thermal actuators are slow and inaccurate. This inaccuracy is especially due to the high sensitivity to small environmental thermal drifts.

In many applications, the thermal effect on piezoelectric actuators has been considered as unwanted disturbance that drastically decreases the accuracy. Therefore, the literature proposes suitable controllers for rejecting it [15] [16]. In this paper, we propose to combine the thermal effect and the piezoelectricity to develop a new actuation concept, called hybrid thermo-piezoelectric. The aim is to benefit from the high resolution and high speed performances of the piezoelectric effect and from the high range of deformation of the thermal actuation. In order to understand the behavior of the actuator, a dynamic model is proposed. The developed model can be used for behavior analysis, design improvement and control design.

The paper is organized as follows. In section-II, we present the new hybrid actuator. Section-III is dedicated to the modeling of the thermal part while section-IV the modeling of the piezoelectric part. Finally, additional experiments and discussions conclude the paper.

FEMTO-ST Institute, UMR CNRS 6174 - UFC / ENSMM / UTBM
Automatic Control and Micro-Mechatronic Systems depart., AS2M
24, rue Alain Savary
25000 Besançon - France
{mrakoton,alex.ivan}@femto-st.fr
Paper type: short paper. First submission: July 2009.

II. Presentation of the new hybrid thermo-piezoelectric actuator

This section presents the principle of the proposed actuator.

A. Principle

The principal actuator is a unimorph piezoelectric cantilever (piezocantilever) which is made up of one PZT-layer (Lead-Zirconnate-Titanate piezoceramic) and one passive layer (Copper) (Fig. 1-a). When an electrical voltage is applied, the PZT-layer expands/contracts resulting a bending δ of the whole cantilever (Fig. 1-b). Furthermore, when a temperature variation is applied, the two layers expands/contracts with different amplitudes as they do not have the same thermal expansion coefficients and a bending is also obtained (Fig. 1-c). This bending represents the output of the actuator.

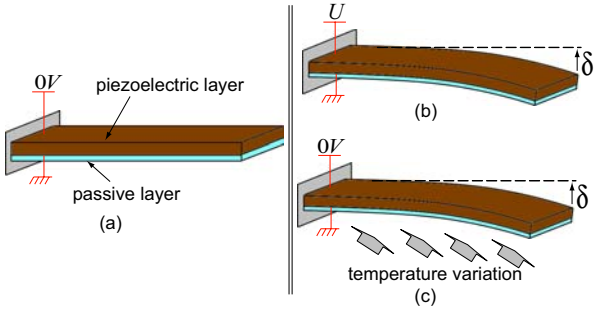

Fig. 1. (a) Unimorph piezocantilever. (b) Piezoelectric actuation. (c) Thermal actuation.

To provide the temperature variation, we propose to use a Peltier module, also called Thermo-Electric-Cooler device (TEC-device). It transforms the electrical current at its input into a heat flux and therefore a temperature change at its surface. Its main advantage is the easiness of control: use of electrical excitation and possibility to reverse heating into cooling. Therefore, by providing either positive or negative current, we can obtain a positive or negative direction of the cantilever deflection. The TEC-device has two sides that will be called "actuator" face and "cooler" face. The piezocantilever is in contact with the actuator face and a cooling block is connected to the cooler face. Fig. 2 presents the CAD drawing of the designed hybrid actuator. The different geometrical characteristics are listed in Table I.

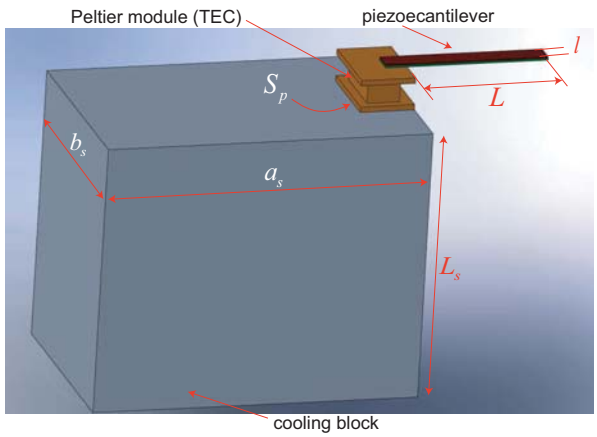

Fig. 2. CAD drawing of the hybrid micro-actuator.

TABLE I

Geometrical characteristics.

Symbol	title	value
L_s	length of the cooling block	$25mm$
a_s	width of the cooling block	$38mm$
b_s	thickness of the cooling block	$20mm$
S_p	area of the TEC-device	$8 \times 5mm^2$
L	active length of the actuator	$15mm$
l	width of the actuator	$2mm$
e_{pzt}	thickness of the PZT-layer	$0.2mm$
e_{cop}	thickness of the Copper-layer	$0.1mm$
e	total thickness	$= e_{pzt} + e_{cop}$

B. Prototype and experimental setup

Fig. 3 shows the prototype of the developed micro-actuator and the experimental setup. An optical sensor (*Keyence-2420*) having a resolution up to $10nm$ and a range of $\pm 200\mu m$ is used to measure the deflection of the piezocantilever. The temperatures at the actuator face of the TEC-device and at the piezocantilever's tip are measured with miniature NTC (Negative Temperature Coefficient) thermistors. A computer, a dSPACE board, a HV (high voltage) and a current amplifier are used to provide the input voltage of the piezocantilever and the input current of the TEC-device, and to acquire the measurements. Finally, we use the Matlab-Simulink ™ software to manage the acquisition and the control program.

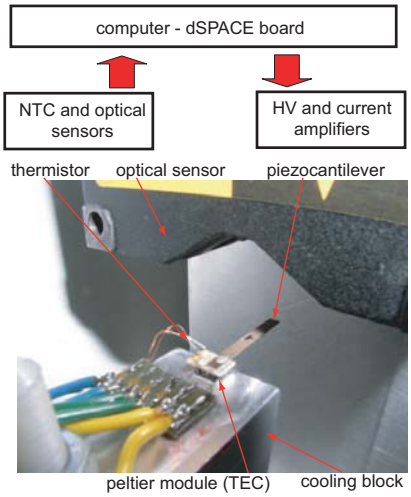

Fig. 3. The data acquisition block diagram and the experimental setup.

C. Block diagram of the micro-actuator

The output of the hybrid actuator is the deflection δ of the piezocantilever. There are two input control signals: the voltage U directly applied to the piezoactuator and the current i applied to the TEC-device. Let T_{act0} denote the temperature at the actuator face of the TEC-device, i.e. at the clamped end $x = 0$ of the piezocantilever. Furthermore, let T_{actL} denote the temperature at the tip of the cantilever (at $x = L$). The temperature T_{act0}, and therefore the temperature T_{actL}, changes when the current i is applied. The temperature inside the piezocantilever also changes and according to the thermal

bimorph principle the deflection is obtained. Fig. 4 sums up the block diagram of the micro-actuator. In the next sections,

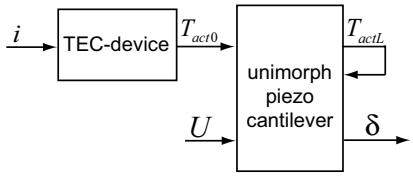

Fig. 4. Systemic scheme of the hybrid thermo-piezoelectric actuator.

first we will model the electrothermal functioning, i.e. from the current i to the temperatures T_{act0} and T_{actL}. Afterwards, we will model the mechanical part, i.e. the deflection versus the input voltage U and versus the temperatures. Finally, we will provide the complete governing equations of the hybrid micro-actuator.

III. Modeling of the Electrothermal Functioning

The aim of this section is to provide the dynamic modeling of the thermal behavior of the hybrid actuator. While the input is the current i of the TEC-device, the output will be the temperatures T_{act0} and T_{actL} of the piezocantilever. For that, we propose to use the thermal network approach. Thermal network is a relatively simple but powerful tool for simulating thermal systems [17]. It is simple and efficient to model several connected subsystems. Thermal network is based on the analogy between thermal and electrical models. A heat flow Q is equivalent to an electrical current, a temperature difference ΔT to a voltage, and a thermal resistance R_{th} to an electrical resistance.

We first give the electrical equivalences of the cooling block, the TEC-device and the piezocantilever separately. Afterwards, we combine them and give the whole model of the electrothermal behavior.

A. The cooling block

To model the cooling block, we start from the network model of a beam structure with rectangular cross-section.

1) Thermal network model of a beam structure: consider a beam structure, with dimensions $L_b \times l_b \times e_b$, along which the heat transfer involves a combination of conduction and convection effects (Fig. 5-a). In the figure, Q_1 and Q_2 are the heat flows through the two terminal surfaces, T_1 and T_2 are the respective temperatures, and a heat convection Q_h takes place from all other surfaces in contact with the external fluid (air) whose temperature is T_a. *Lopez-Walle et al.* [18] demonstrated that the dynamic thermal network of the beam structure is as shown in Fig. 5-b, where the conduction thermal resistance is $R = \frac{L_b}{kS_b}$, the convection thermal resistance is $R_v = \frac{2}{h_{air}P_bL_b}$ and the thermal capacitor is $C = \frac{\rho C_p S_b L_b}{2}$. We have: $P_b = 2\,(e_b + l_b)$ as the lateral perimeter and $S_b = e_b l_b$ as the section of the beam. The physical parameters are the thermal conductivity k, the mass-specific heat capacity C_p, the air heat transfer coefficient h_{air} and the density ρ.

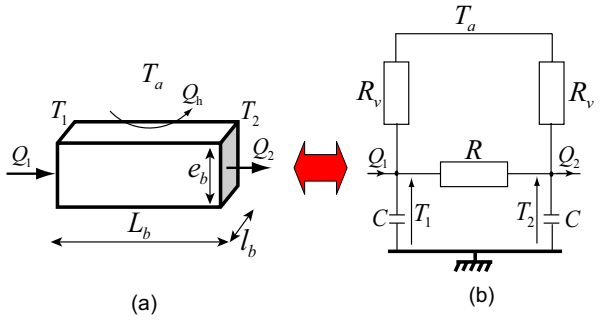

Fig. 5. (a) A beam structure. (b) Dynamic thermal network of the beam.

2) Thermal network model of the cooling block: the bottom surface of the cooling block is placed on a heat insulator (zero heat flow) (Fig. 6-a). At the second terminal surface (frontal surface), only a small area S_p is connected to the TEC-device. In fact, there is a small adhesive (glue) thickness layer $l_c = 0.1mm$ between the cooler face of the cooling block and the TEC-device. Therefore, the heat flow Q_r traverses this thin film. Two surfaces are submitted to a heat convection: the lateral surface submitted to Q_{vs} and the frontal surface submitted to Q_{vsf}. Applying the previous beam analysis, we

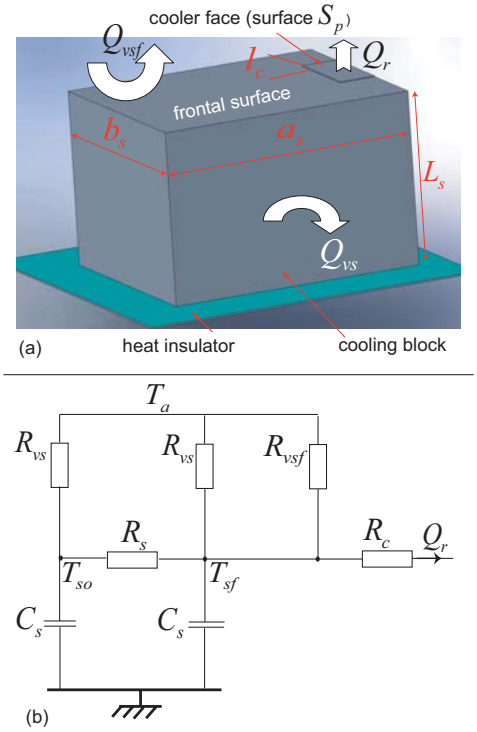

Fig. 6. Analysis of the cooling block.

obtain the Fig. 6-b where R_{vs} and R_{vsf} are the lateral and frontal convection thermal resistances respectively, R_s is the conduction thermal resistance and C_s the heat capacity of the cooling block. The element R_c represents the conduction thermal resistance of the thickness l_c. The signals T_{so} and T_{sf} are the temperatures of the block at the two terminal surfaces.

We have:

$$R_{vs} = \frac{2}{h_{air} P_s L_s}, \qquad R_{vsf} = \frac{2}{h_{air}(b_s a_s - S_p)}$$
$$R_s = \frac{L_s}{k_s S_s}, \qquad R_c = \frac{L_c}{k_s S_p}, \qquad C_s = \frac{\rho_s C_{ps} S_s L_s}{2} \tag{1}$$

where k_s is the thermal conductivity, C_s is heat capacity and ρ_s is the density of aluminium. $S_s = a_s b_s$ is the section and $P_s = 2(e_s + l_s)$ is the perimeter of the block.

B. The TEC-device

A TEC-device is characterized by the two following symmetrical equations:

$$Q_c = -\alpha T_c i + \frac{R_p}{2} i^2 + kp\,(T_h - T_c)$$
$$Q_h = -\alpha T_h i + \frac{R_p}{2} i^2 - kp\,(T_h - T_c) \tag{2}$$

where:

- Q_c and Q_h are the heat flow at the cooler face and actuator face respectively,
- T_c and T_h are the temperature values of the two respective faces,
- α is the Peltier coefficient,
- k_p is the device thermal conductivity,
- and R is the internal electrical resistance of the TEC-device.

Based on (Eq. 2), *Selliger et al.* [19] proposes a thermal network as presented in Fig. 7. In this scheme, the Peltier effect is represented by the flow source $P_s = \alpha T_c i$, the Joule effect by $P_{J/2} = \frac{R_p}{2} i^2$ and a thermal resistance term by $R_{th} = \frac{1}{k_p}$.

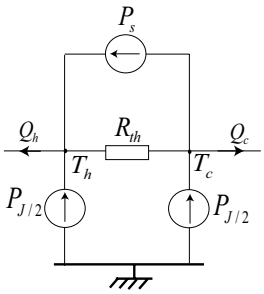

Fig. 7. Thermal network of a TEC-device.

C. The piezocantilever

The piezocantilever consists of two materials: the PZT-layer and the copper-layer. The thickness of the interface (glue) between the two layers is considered to be negligible. To give the thermal network, we first remind the case of parallel and serial structures.

1) Thermal network of parallel and serial structures : consider a heat flow Q_1 that traverses two parallel materials m_1 and m_2 as pictured in Fig. 8-a. The equivalent thermal resistance is the shunt of the two elementary thermal resistances of the materials [17] (Fig. 8-b). To account the dynamic part, we add the capacitors as preconized in Fig. 5-b. If we consider now two materials which appear in cascade face to a convection flow (Fig. 8-c), then their two resistances will also be in cascade [17](Fig. 8-d).

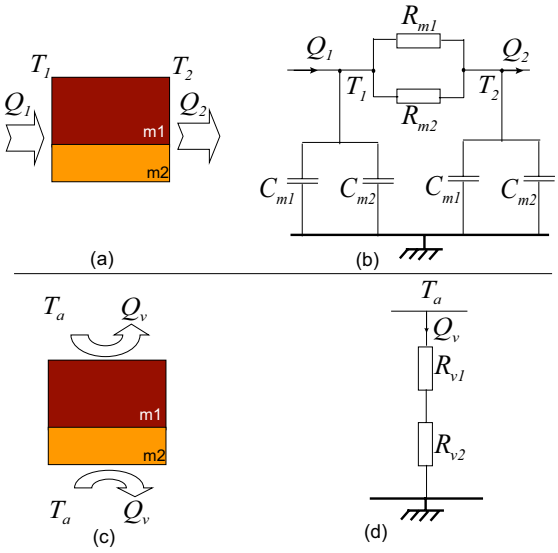

Fig. 8. Parallel and serial thermal structures.

2) Thermal network of the piezocantilever: Fig. 9-a pictures the piezocantilever under different heat flows. The flow Q_c comes from the TEC-device and Q_{va1} and Q_{va2} are the convection flows on the lateral surface and at the extremity respectively.

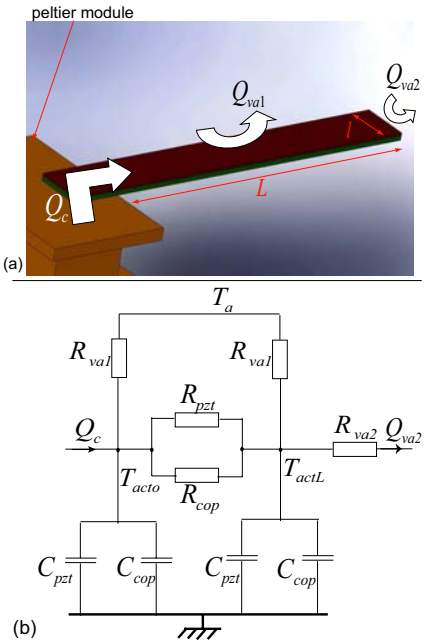

Fig. 9. Thermal network of the piezocantilever.

The thermal network of the piezocantilever is given by Fig. 9-b. R_{va1} is the convection thermal resistance which is related to Q_{va1}. R_{va2} is the convection thermal resistance which resists to the flow Q_{va2}. The final conduction thermal resistor and capacitor of the piezocantilever is made up of the

piezolayer and of the copper-layer in parallel. We have:

$$\begin{array}{lll} R_{pzt}=\frac{L}{k_{pzt}\cdot S_{pzt}}, & R_{cop}=\frac{L}{k_{cop}\cdot S_{cop}}, & R_{va1}=\frac{2}{h_{air}P_{act}L} \\ R_{va2}=\frac{2}{h_{air}S_{act}}, & \rho_{pzt}C_{ppzt}S_{pzt}L, & C_{cop}=\frac{\rho_{cop}C_{pcop}S_{cop}L}{2} \end{array} \tag{3}$$

where k_{pzt} and k_{cop} are the thermal conductivities, C_{ppzt} and C_{pcop} the heat capacities, ρ_{pzt} and ρ_{cop} the densities of PZT and copper respectively. On the other hand, $S_{pzt}=e_{pzt}l$ and $S_{cop}=e_{cop}l$ are the sections of the piezolayer and the copper-layer respectively. Finally, $P_{act}=2\,(l+e)$ and $S_{act}=S_{pzt}+S_{cop}=el$ are the perimeter and cross-section of the actuator.

D. Final model of the electrothermal functioning

Assemblying the previous different elements, we obtain the thermal network of the hybrid actuator as pictured in Fig. 10. In the figure, we define:

$$\begin{cases} R_{va1//2}=\frac{R_{va1}R_{va2}}{(R_{va1}+R_{va2})}, & R_{vs//f}=\frac{R_{vs}R_{vf}}{(R_{vs}+R_{vf})} \\ C_{act}=C_{pzt}+C_{cop} \end{cases} \tag{4}$$

Applying *Kirchhoff* laws to the circuit of Fig. 10, we obtain the four governing equations of the thermal functioning:

$$T_a=R_{vs}C_s\frac{dT_{so}}{dt}+\left(\frac{R_{vs}+1}{R_s}\right)T_{so}-\frac{R_{vs}}{R_s}T_{sf} \tag{5}$$

$$\begin{array}{l} T_a=R_{vs//f}C_s\frac{dT_{sf}}{dt}+\left(\frac{R_{vs//f}}{(R_{th}+R_c)}+\frac{R_{vs//f}}{R_s}+1\right)T_{sf} \\ -\frac{R_{vs//f}}{R_s}T_{so}+\left(\frac{R_{vs//f}R_c}{R_{th}(R_{th}+R_c)}-\frac{R_{vs//f}}{R_{th}}\right)T_{acto} \\ +\left(\frac{R_{vs//f}R_c}{(R_{th}+R_c)}-R_{vs//f}\right)P_s+\left(\frac{R_{vs//f}R_c}{(R_{th}+R_c)}-R_{vs//f}\right)P_{j/2} \end{array} \tag{6}$$

$$\begin{array}{l} T_a=R_{va1}C_{act}\frac{dT_{acto}}{dt}+\left(\frac{R_{va1}}{R_{act}}+\frac{R_{va1}}{R_{th}}-\frac{R_{va1}R_c}{R_{th}(R_{th}+R_c)}\right)T_{acto} \\ -\frac{R_{va1}}{R_{act}}T_{actL}-\frac{R_{va1}}{(R_{th}+R_c)}T_{sf}+\left(R_{va1}-\frac{R_{va1}R_c}{(R_{th}+R_c)}\right)P_s \\ -\left(R_{va1}+\frac{R_{va1}R_c}{(R_{th}+R_c)}\right)P_{j/2} \end{array} \tag{7}$$

$$\begin{array}{l} T_a=R_{va1//2}C_{act}\frac{dT_{actL}}{dt}-\frac{R_{va//2}}{R_{act}}T_{acto} \\ +\left(\frac{(R_{va1//2}+R_{act})}{R_{act}}\right)T_{actL} \end{array} \tag{8}$$

IV. Modeling of the Piezoelectric and Thermomechanical Functioning

A. Constitutive equations in static regime

Smits and Choi [20] derive the static constituent equation of a rectangular unmiorph structure containing one piezolayer and one passive layer. The deflection δ at the tip was formulated versus the applied voltage U and versus the temperature variation T:

$$\delta=d_pU+f_sT \tag{9}$$

where the piezoelectric coefficient is $d_p=-\frac{3Ad_{31}BL^2}{K}$ and the thermoelectric coefficient is $f_s=\frac{3ABL^2\Delta\alpha}{K}$, with:

$$\begin{array}{l} A=s_{11}^c s_{11}^p\left(s_{11}^c h_p+s_{11}^p e_c\right), \qquad B=\frac{e_c(e_p+e_c)}{\left(s_{11}^c e_p+s_{11}^p e_c\right)} \\ K=\left(s_{11}^c\right)^2(e_p)^4+\left(s_{11}^p\right)^2(e_c)^4+4s_{11}^c s_{11}^p e_c(e_p)^3 \\ +4s_{11}^c s_{11}^p e_p(e_c)^3+6s_{11}^c s_{11}^p(e_c)^2(e_p)^2 \end{array} \tag{10}$$

and where d_{31} is the transverse piezoelectric coefficient of PZT, s_{11}^p and s_{11}^c are the axial elastic coefficients of PZT and copper respectively, and $\Delta\alpha=\alpha_{pzt}-\alpha_{cop}$ is the difference of their thermal expansion coefficients.

B. Introduction of the dynamic part

Two dynamic parts can be introduced in the model of (Eq. 9): one for the piezoelectric (electromechanical) term and one for the thermomecanichal term, such as: $\delta=d_pUD(s)+f_sTD_T(s)$. The Laplace variable is denoted by s.

Piezoelectric dynamic part $D(s)$ is of interest because it could be used to control and improve the performances of the fine positioning mode. Thermomechanical dynamic part $D_T(s)$ is not easy to characterize and identify. In fact, it is impossible to apply pure canonical temperature signals T (impulse, step, etc.) to perform that. Assuming that the thermomechanical dynamic part $D_T(s)$ is very rapid compared to the electrothermal dynamic model in (Eq. 5)-(Eq. 8), the latter dominates in the transfer between current i and output deflection δ. So we shall neglect $D_T(s)$ in the electrothermo-mechanical functioning and we will finally use:

$$\delta=d_pUD(s)+f_sT \tag{11}$$

C. Temperature gradient in the the piezocantilever

In model (Eq. 11), T is considered to be uniform all accross the piezocantilever. Nevertheless, the thermal model in (Eq. 5)-(Eq. 8) points out that the temperatures T_{acto} and T_{actL} could be distinct. For a more analysis, we capture the temperature field of the piezocantilever using a IR camera. Fig. 11 present the images when the temperature at the actuator face of the TEC-device is $19[^oC]$ and then $43[^oC]$. These results show that the temperature gradient inside the piezocantilever is negligible except for the boundary between the TEC-module and the cantilever. Thus, we can assume that the temperature is T_{actL} all along it. In addition, as the temperature is uniform inside the piezocantilever, whatever the side (PZT or copper) glued on the TEC-device is, the performances are similar. The final model of the deflection of the piezocantilever is:

$$\delta=d_pUD(s)+f_s(T_{actL}-T_a) \tag{12}$$

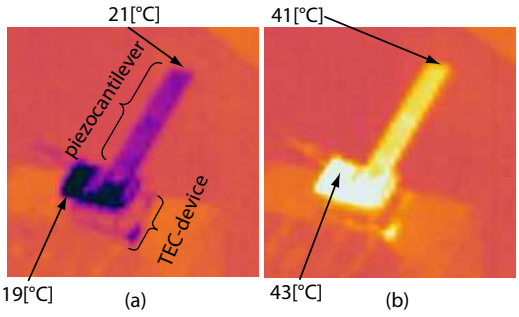

Fig. 11. The thermal images of the piezocantilever using an IR camera.

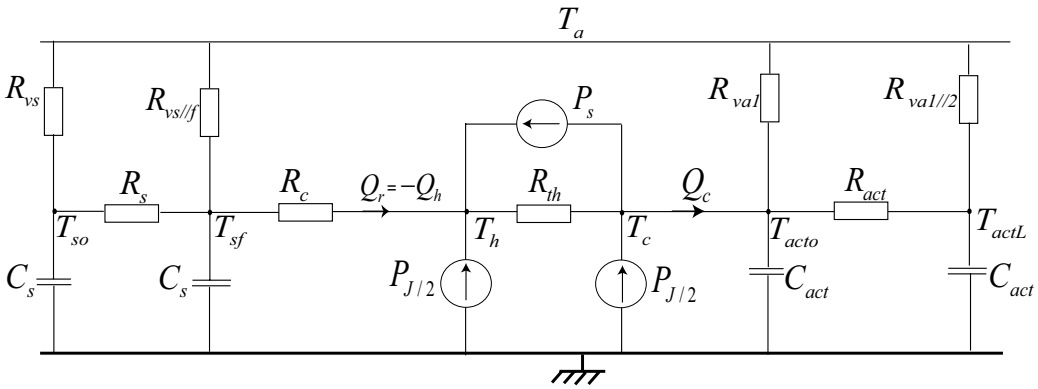

Fig. 10. Thermal network of the hybrid actuator.

V. Final Model and Experiments

A. The final governing model

The final model includes the electrothermal dynamic model in (Eq. 5)-(Eq. 8) and the dynamic model of the piezoelectric actuator in (Eq. 12). The dynamic part $D(s)$ can be experimentally identified. Re-arranging the different equations we have:

$$\begin{cases} \frac{dT_{so}}{dt} = \frac{1}{\tau_s}T_{sf} - \frac{b_{so}}{\tau_s}T_{so} + \frac{1}{\tau_{vs}}T_a \\ \frac{dT_{sf}}{dt} = \frac{1}{\tau_s}T_{so} - \frac{c_{sf}}{\tau_{vs//f}}T_{sf} - \frac{c_{acto}}{\tau_{vs//f}}T_{acto} - \frac{c_{ps}}{\tau_{vs//f}}T_{acto}i \\ \quad -\frac{c_{j/2}}{\tau_{vs//f}}i^2 + \frac{1}{\tau_{vs//f}}T_a \\ \frac{dT_{acto}}{dt} = \frac{1}{\tau_{act}}T_{actL} - \frac{d_{acto}}{\tau_{rva1}}T_{acto} + \frac{d_{sf}}{\tau_{rva1}}T_{sf} - \frac{d_{ps}}{\tau_{rva1}}T_{acto}i \\ \quad +\frac{d_{j/2}}{\tau_{rva1}}i^2 + \frac{1}{\tau_{rva1}}T_a \\ \frac{dT_{actL}}{dt} = \frac{1}{\tau_{act}}T_{act0} - \frac{e_{actL}}{\tau_{rva1//2}}T_{actL} + \frac{1}{\tau_{rva1//2}}T_a \\ \delta = d_pUD(s) + f_s(T_{actL} - T_a) \end{cases} \tag{13}$$

with, for the first equation

$$\tau_s = R_sC_s, \quad \tau_{vs} = R_{vs}C_s, \quad b_{so} = \frac{(R_{vs}+R_s)}{R_{vs}} \tag{14}$$

for the second equation

$$\begin{aligned} \tau_{vs//f} &= R_{vs//f}C_s \\ c_{sf} &= \left(\frac{R_{vs//f}}{(R_{th}+R_c)} + \frac{R_{vs//f}}{R_s} + 1\right) \\ c_{acto} &= \left(\frac{R_{vs//f}R_c}{R_{th}(R_{th}+R_c)} - \frac{R_{vs//f}}{R_{th}}\right) \\ c_{ps} &= \alpha\left(\frac{R_{vs//f}R_c}{(R_{th}+R_c)} - R_{vs//f}\right) \\ c_{pj/2} &= \frac{R_p}{2}\left(\frac{R_{vs//f}R_c}{(R_{th}+R_c)} - R_{vs//f}\right) \end{aligned} \tag{15}$$

for the third equation

$$\begin{aligned} \tau_{act} &= R_{act}C_{act}, \quad \tau_{rva1} = R_{rva1}C_{act} \\ d_{acto} &= \left(\frac{R_{rva1}}{R_{act}} + \frac{R_{rva1}}{R_{th}} - \frac{R_{va1}R_c}{R_{th}(R_{th}+R_c)} + 1\right) \\ d_{sf} &= \frac{R_{va1}}{(R_{th}+R_c)}, \quad d_{ps} = \alpha\left(R_{va1} - \frac{R_{va1}R_c}{(R_{th}+R_c)}\right) \\ d_{pj/2} &= \frac{R_p}{2}\left(R_{va1} + \frac{R_{va1}R_c}{(R_{th}+R_c)}\right) \end{aligned} \tag{16}$$

and for the fourth equation

$$\tau_{rva1//2} = R_{rva1//2}C_{act}, \quad e_{actL} = \left(1 + \frac{R_{va1//2}}{R_{act}}\right) \tag{17}$$

Table II resumes the physical properties that will be used for simulation.

TABLE II
Physical properties.

Symbol	title	value
Air:		
h_{air}	convection thermal coefficient	$30W/(m^2K)$
Cooling block (alumina):		
ρ_s	density	$2701kg/m^3$
C_{ps}	thermal capacity	$902J/(kgK)$
k_s	thermal conductivity	$222W/(m^oK)$
Passive layer (copper):		
ρ_c	density	$7135kg/m^3$
C_{pc}	thermal capacity	$386J/(kgK)$
k_c	thermal conductivity	$381.5W/(mK)$
α_{cop}	thermal expansion	17×10^{-6}
s^c_{11}	axial elastic constant	$9.1 \times 10^{-12}m^2/N$
TEC-device:		
α	Peltier coefficient	$12 \times 10^{-3}V/K$
k_p	thermal capacity	$12 \times 10^{-3}J/(kgK)$
PZT (-5H):		
ρ_{pzt}	density	$7500kg/m^3$
C_{ppzt}	thermal capacity	$420J/(kgK)$
k_{pzt}	thermal conductivity	$138W/(mK)$
d_{31}	transverse piezoelectroc coefficient	$-100 \times 10^{-12}m/V$
s^p_{11}	axial elastic constant	$15 \times 10^{-12}m^2/N$
α_{cop}	thermal expansion	3.3×10^{-3}

B. Electrothermal experimental result

The first experiments concern the electrothermal functioning which links the applied current i and the different temperatures. We are especially interested in the temperature T_{act0} of the TEC-device at $x = 0$ of the piezocantilever. A sine input with $i = 0.1[A]$ of amplitude is applied to the TEC-device. The frequency is chosen to be very low ($0.001[Hz]$) in order to avoid the influence of the dynamic part to the shape of the static characteristics, i.e. due to the phase lag. The results are compared with the simulation of the developed model and show that the latter is accurate (Fig. 12). Afterwards, a series of steps at different values ($i = 0.1[A]$, $i = 0.05[A]$ and $i = 0.025[A]$) are applied to the TEC-device. Fig. 13 pictures the experimental and model simulation results. It also shows

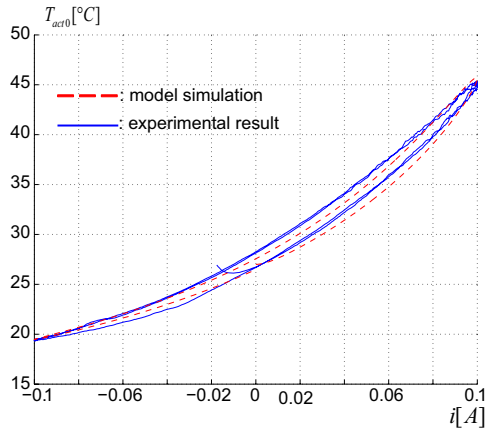

Fig. 12. Static characteristics between the applied current $i[A]$ and the temperature $T_{act0}[°C]$ at $x = 0$ of the piezocantilever.

that both the transient part and the final value of the model simulation well fit to the experiments.

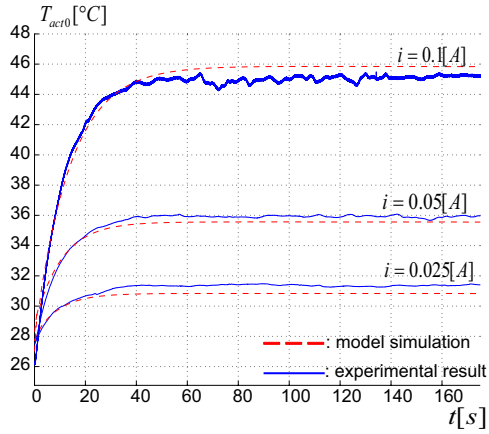

Fig. 13. Response of the temperature $T_{act0}[°C]$ at $x = 0$ to step input.

C. Thermomechanical experimental result

The next experiment concerns the deflection δ of the piezocantilever versus the temperature variation: the thermomechanical behavior. For that, we impose $U = 0$ so that $\delta = f_s\left(T_{actL} - T_a\right)$ for the last equation of the model in (Eq. 13). Fig. 14 gives the (static characteristic) comparison between the model (linear dashed-plot) and the experimental result for the deflection δ versus the temperature T_{actL}. It shows that the linear model does not reflect the real characteristics of the actuator. We then propose a polynomial model: $\delta_{sim} = \sum_{i=1}^{n_i} a_i \left(T_{actL} - T_a\right)^i$, such as $a_1 = f_s$. The identification of the parameters a_i is based on the following optimization problem:

$$\begin{cases} \varepsilon_{\min} = \min\limits_{a_i \in \mathbb{R}^{n_i}} \left(\sum\limits_{k=0}^{N} \left(\delta(k) - \delta_{sim}(k)\right)^2 \right) \\ \delta_{sim}(k) = \sum\limits_{i=1}^{n_i} a_i \left(T_{actL} - T_a\right)^i (k) \end{cases} \tag{18}$$

where N is the data length. Using Matlab ™ and several choices of model-order n_i, it appeared that the modeling error $\varepsilon_{\min}$ did not decrease substantially when n_i is greater than four. Therefore, we choose:

$$\delta = \sum_{i=1}^{4} a_i \left(T_{actL} - T_a\right)^i \tag{19}$$

with $a_4 = -0.00169$, $a_3 = 0.04056$, $a_2 = -0.32233$ and $a_1 = f_s$. The simulation result, presented by star-plot in Fig. 14, well fits to the experimental results.

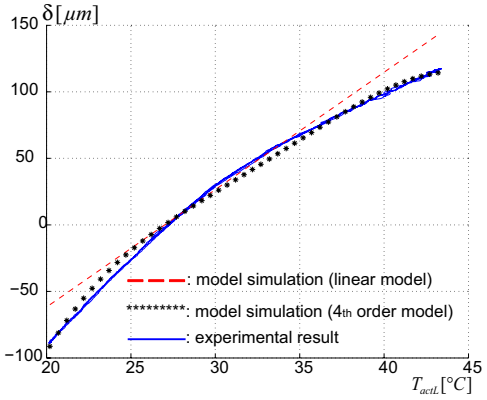

Fig. 14. Actuator deflection δ versus the temperature T_{actL} at $x = L$.

D. Piezoelectric experimental result

In this part, the piezoelectric characteristic $\delta = d_p U D(s)$ in model (Eq. 13) is analyzed.

1) Static characteristics: we first analyze the static behavior of the piezocantilever. To perform that, a sine input voltage of amplitude $U = 40[V]$ is applied. The frequency is chosen to be low (here we choose $f = 0.1[Hz]$) to avoid the influence of the dynamic part $D(s)$ [11]. The experimental results (Fig. 15-solid line) and the simulation of the model $\delta = d_p U$ (Fig. 15-dashed line) show that a linear model is not accurate enough to capture the static behavior of the piezocantilever. In fact, piezoelectric materials, especially ceramics, are strongly subjected to hysteresis when the applied electrical fields is relatively high. Therefore, we propose to use a nonlinear model.

There are different models of hysteresis used to characterize smart materials: the Preisach [22], the Prandtl-Ishlinskii [23] [24] and the Bouc-Wen models [25]. The Prandtl-Ishlinski model (PI-model) is notably appreciated for simplicity of its implementation and ease of obtaining a control law [26].

In the PI approach, a hysteresis is modeled by the sum of many elementary hysteresis operators, called play operators. Each play operator, denoted by $\gamma_i(.)$, is characterized by a threshold r_i and a weighting w_i [27]. So, instead of $\delta(t) = d_p U(t)$, we have:

$$\begin{aligned} \delta(t) &= \sum_{i=1}^{n_{hyst}} \gamma_i \left(U(t)\right) \\ &= \sum_{i=1}^{n_{hyst}} w_i \cdot \max\left\{U(t) - r_i, \min[U(t) + r_i, \delta(t^-)]\right\} \end{aligned} \tag{20}$$

where $\delta(t^-)$ indicates the value of the output at precedent time and n_{hyst} the number of play operators. The identification of the parameters r_i and w_i, well described in [26], is done using the maximum operating input range $U = 40[V]$. For a trade-off between the accuracy and the simplicity, we choose a number $n_{hyst} = 15$. The identified model is pictured in Fig. 15-star plot. The figure clearly shows that the PI model is more suitable to capture the static behavior of the piezocantilever than the linear model.

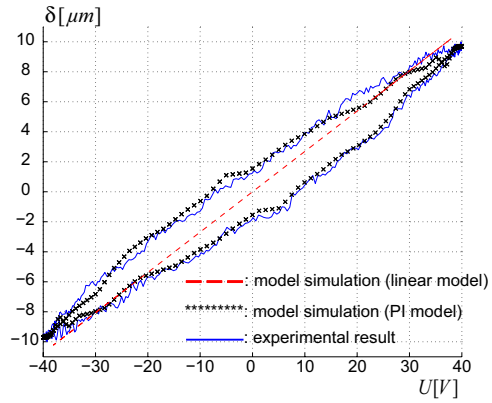

Fig. 15. Hysteresis between the applied voltage U and the deflection δ.

2) Dynamic characteristics: we now identify the dynamic part $D(s)$. For this purpose, a step input of amplitude $U = 40V$ is applied. Using ARMAX (Auto Regressive and Moving Average eXogenous) method [28], it is shown that a third order model well captures the transient part. The simulated model and the experimental results are pictured in Fig. 16, and the model is:

$$D(s) = \frac{\delta}{U} = \frac{102\left(s^2 + 2.58 \times 10^4 s + 2.4 \times 10^8\right)}{(s + 1274)\left(s^2 + 34.1s + 1.9 \times 10^7\right)} \quad (21)$$

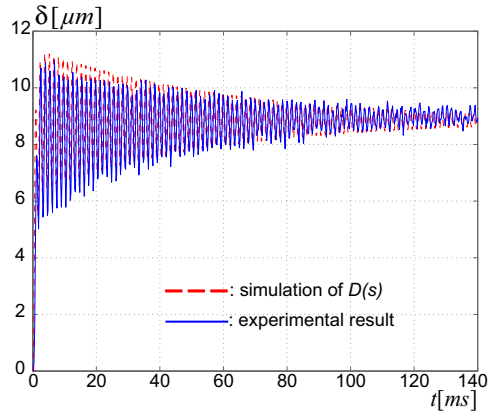

Fig. 16. Resulting deflection δ when using a step input $U = 40[V]$.

E. Modeling overview and discussions

The four first equations of the developed model in (Eq. 13) well fit to the experimental results. These equations refer to the electrothermal functioning of the hybrid actuator. The last equation of (Eq. 13), which corresponds to the piezoelectric and thermomechanical behaviors, is not accurate enough. This equation, developed in [20], does not take into account the ferroelectric materials nonlinearities such as the hysteresis. Therefore, we have proposed a polynomial model for the thermomechanical part and a Prandtl-Ishlinskii (PI) hysteresis model for the piezoelectric (electromechanical) one. Contrarily to the electrothermal equations which are based on physical parameters, the proposed nonlinear model of the themomechanical and piezoelectric sub-systems is with lumped parameters. Using the previous section, the piezocantilever equation (last equation in (Eq. 13)) is therefore replaced with:

$$\delta(t) = \left(\sum_{i=1}^{n_{hyst}} \gamma_i\left(U(t)\right)\right) D(s) + \sum_{i=1}^{n_i} a_i \left(T_{actL}(t) - T_a\right)^i \quad (22)$$

As presented in (Eq. 13) and (Eq. 22), the output deflection δ is dependent on the ambient temperature T_a. However, if T_a changes, the temperatures T_{act0} and T_{actL} of the TEC-device and of the piezocantilever (when $i = 0[A]$) also change as these elements are exhibited in the air, and as a result the initial deflection still remains zero.

Fig. 17 gives a synthesis of the modeling aspect in the form of detailed block diagram that presents the connections between the different signals of the actuator. In the figure, the electrothermal functioning of the actuator is described by the Peltier/cooling block and the thermal bimorph model blocks. They provide the temperature T_{actL} that corresponds to the thermal actuation of the piezocantilever. The *polynomial* and the *PI-hyst* blocks describe the thermomechanical and the piezoelectrical functioning respectively.

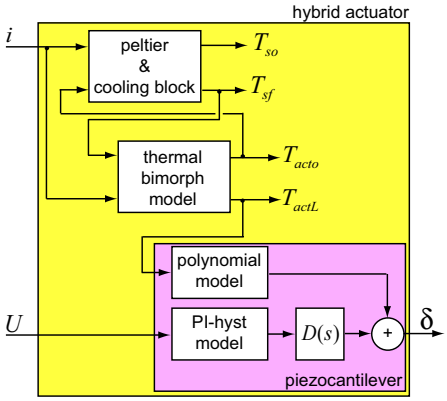

Fig. 17. Detailed block diagram of the hybrid actuator.

The developed model is of great interest from the point of view of performances improvement. The dynamic model as in (Eq. 13) and (Eq. 22) and summarized in Fig. 17 does not only allow us to understand the behavior of the actuator, but also constitutes a starting point for the design of a controller to improve the dynamics and the accuracy performances. Such performances are necessary for micromanipulation and microassembly tasks where the developed actuator can be used as microgrippers. This application requires the use of actuators with both the high range (more than the hundred of microns) and the high resolution (better than the micron). Table III

gives a general summary of performances of the proposed actuator compared to classical unimorph piezocantilever and to a thermal bimorph having the same dimensions and materials components (PZT and copper) as well as operating input ranges ($U = 40[V]$ and temperature variation: $20[^oC]$). The resolution of the thermal bimorph actuator depends on the temperature source element (using the TEC-device, we obtain $\approx 1\mu m$).

TABLE III

Performances summary.

Actuator	bandwidth	Resolution	range
classic piezo-cantilever	$> 600Hz$	better than $100nm$	$\approx 10\mu m$
classic thermal bimorph	$\approx 4mHz$	$\approx 1\mu m$	$> 100\mu m$
hybrid actuator	coarse mode: $\approx 4mHz$ fine mode: $> 600Hz$	better than $100nm$	$> 110\mu m$

VI. Conclusion

The aim of this paper was the presentation, development and modeling of a new hybrid actuator. The actuator, based on a piezocantilever, combines the piezoelectric effect and the thermal bimorph principle. The main advantage lies in the combination of the high range of displacement from the thermal actuation and of the high resolution from the piezoelectric actuation. To apply the temperature variation, the piezocantilever was embedded on a Peltier module (TEC-device). A model of the hybrid actuator was developed and validated by experimental results. The thermal network was used to model the thermal dynamic behavior because of its ease to connect subsystems. To model the piezocantilever's deflection, *Smits and Choi*'s linear model was first used. However, due to the nonlinearities aspect of the piezomaterial, we have proposed a polynomial and a Prandtl-Ishlinskii (PI) models for the thermomechanical and piezoelectric terms respectively. The developed model can be used for behavior analysis, design optimization and control design.

Acknowledgment

This work is supported by the EU FP7SP3-People Program under Grant No: PIEF-GA-2008-219412: MicroPAdS. It was partially presented in [29] and is subjected to a patent pending.

References

[1] W. Lin and W. J. Chen, "Fiber assembly of MEMS optical switches with U-groove channels", IEEE Transactions on Automation Science and Engineering (TASE), Vol.5(2), pp.207-215, 2008.

[2] C. Clévy, A. Hubert and N. Chaillet, "Flexible Micro-Assembly System Equiped with an Automated Tool Changer", Springer Journal of Micro-Nano Mechatronics (J-MNM), Vol.4(1), pp.59-72, 2008

[3] A. N. Das, J. Sin, D. O. Popa and H. E. Stephanou, "On the Precision Alignment and Hybrid Assembly Aspects in Manufacturing of a Microspectrometer", IEEE Conf. on Autom. Science and Engin., 2008.

[4] Lu Zhe, P. C. Y. Chen, Nam Joo Hoo, Ge Ruowen and Lin Wei, "A Micromanipulation System for Automatic Batch Microinjection", IEEE Int. Conf. on Robotics and Autom., pp.3134-3135, Roma Italy 2007.

[5] M. Boukallel, M. Girot and S. Régnier, "Characterization of cellular mechanical behavior at the microscale level by a hybrid force sensing device", Elsevier Journal of the Mechanical Behavior of Biomedical Materials (J-MBBM), pp.297-304, October 2009.

[6] D. J. Capparelli, M. I. Frecker, T. W. Simpson and A. Snyder, "Design of a PZT bimorph actuator using a metamodel-based approach", ASME Journal of Mechanical Design (J-MD), pp.354-357, 2002.

[7] H. Xinhan, C. Jianhua, W. Min and L. Xiadong , "A piezoelectric bimorph micro-gripper with micro-force sensing", IEEE International Conference on Information Acquisition (ICIA), June-July 2005.

[8] A. Bergander, W. Driesen, T. Varidel, M. Meizoso and J. M. Breguet, "Mobile cm^3-microrobots with tools for nanoscale imaging and micromanipulation", Mechatronics and Robotics Conference (MECHROB), pp.1041-1047, Aachen Germany, September 2004.

[9] Micky Rakotondrabe, Yassine Haddab and Philippe Lutz, "Development, Modeling, and Control of a Micro-/Nanopositioning 2-DOF Stick-Slip Device", IEEE Trans. on Mechatronics, V.14(6), pp:733-745, Dec. 2009.

[10] B. Mokaberi and A. A. G. Requicha, "Compensation of scanner creep and hysteresis for AFM nanomanipulation", IEEE Trans. on Autom. Science and Engin. (TASE), Vol.5(2), pp.197-208, 2008.

[11] M. Rakotondrabe, Y. Haddab and P. Lutz, "Quadrilateral modelling and robust control of a nonlinear piezoelectric cantilever", IEEE Trans. on Control Syst. Tech. (TCST), Vol.17(3), pp.528-539, May 2009.

[12] D. O. Popa and B. H. Kang and J. T. Wen and H. E. Stephanou and G. Skidmore and A. Geisberger, "Dynamic Modeling and Input Shaping of Thermal Bimorph MEMS Actuators", IEEE Int. Conf. on Robotics and Autom., pp.1470-1475, Taipei Taiwan, Sept. 2003.

[13] A. Jain, H. Qu, S. Todd and H. Xie, "A thermal bimorph micromirror with large bi-directional and vertical actuation", Elsevier Sensors and Actuators A (S&A), pp.9-15, 2005.

[14] B. Lopez-Walle, M. Gauthier and N. Chaillet, "Principle of a submerged freeze gripper for microassembly", IEEE Transactions on Robotics (TRO), Vol.24, No4, pp.897-902, 24, 2008.

[15] B. Mokaberi and A. A. G. Requicha, "Drift compensation for automatic nanomanipulation with scanning probe microscopes", IEEE Trans. on Automation Science and Engin. (TASE), Vol.3(3), pp.199-207, 2006.

[16] Micky Rakotondrabe, Cédric Clévy and Philippe Lutz, "H-inf deflection control of a unimorph piezoelectric cantilever under thermal disturbance", IEEE International Conference on Intelligent Robots and Systems (IROS), pp:1190-1197, San Diego CA USA, Oct-Nov 2007.

[17] J. P. Holman, "Heat transfer", McGraw-Hill Book Company, ISBN 0-07-029620-0, 6th edition 1986.

[18] Beatriz Lopez-Walle, Michaël Gauthier and Nicolas Chaillet, "Dynamic modelling for thermal micro-actuators using thermal networks", Elsevier Sensors and Actuators A (S&A).

[19] G. Selliger, J. Stephan and S. Lange, "Hydroadhesive gripping by using peltier effect", ASME International Mechanical Engineering Congress & Exposition (IMECE), pp.3-8, Florida USA, November 2000.

[20] J. G. Smits and W-S. Choi, "Equations of state including the thermal domain piezoelectric and pyroelectric heterogeneous bimorphs", IEEE Ultrasonics Symposium, pp.1035-1038, 1992.

[21] `http://www.comsol.fr/`

[22] A. Dubra and J. Massa and C.l Paterson, "Preisach classical and nonlinear modeling of hysteresis in piezoceramic deformable mirrors", Optics Express, Vol.13, N^o22, pp.9062-9070, 2005.

[23] K. Kuhnen and H. Janocha, "Inverse feedforwrad controller for complex hysteretic nonlinearities in smart-materials systems", Control of Intelligent System, Vol.29, N^o3, 2001.

[24] B. Mokaberi and A. A. G. Requicha, "Compensation of scanner creep and hysteresis for AFM nanomanipulation", IEEE Transactions on Automation Science and Engineering, Vol.5, N^o2, pp.197-208, 2008.

[25] M. Rakotondrabe, "'Bouc-Wen modeling and inverse multiplicative structure to compensate hysteresis nonlinearity in piezoelectric actuators", IEEE Trans. on Automation Science and Engin. (TASE), in press 2011.

[26] M. Rakotondrabe, C. Clévy and P. Lutz, "Complete open loop control of hysteretic, creeped and oscillating piezoelectric cantilevers", IEEE Trans. on Automation Science and Engin. (TASE), DOI 10.1109/TASE.2009.2028617.

[27] M. A. Krasnosel'skii and A. V. Pokrovskii, "Systems with hysteresis", Springer-Verlag, Berlin, 1989.

[28] L. Ljung, "System Identification Toolbox - for use with MATLAB", Matlab User's Guide,1988.

[29] M. Rakotondrabe and I. A. Ivan, "Principle, characterization and control of a new hybrid thermo-piezoelectric microactuator", IEEE Int. Conf. on Robotics and Automation, Anchorage Alaska USA, May 2010.